Normal stress in magnetorheological polymer gel under large amplitude oscillatory shear

Haoming Pang, Lei Pei, Chuanlin Sun, and Xinglong Gong

Citation: Journal of Rheology **62**, 1409 (2018); doi: 10.1122/1.5030952
View online: https://doi.org/10.1122/1.5030952
View Table of Contents: http://sor.scitation.org/toc/jor/62/6
Published by the The Society of Rheology

Normal stress in magnetorheological polymer gel under large amplitude oscillatory shear

Haoming Pang, Lei Pei, Chuanlin Sun, and Xinglong Gong[a)]

CAS Key Laboratory of Mechanical Behavior and Design of Materials, Department of Modern Mechanics, University of Science and Technology of China (USTC), Hefei 230027, Anhui, China

(Received 27 March 2018; final revision received 9 September 2018; published 28 September 2018)

Abstract

In this study, the normal stress in magnetorheological polymer gel (MRPG) under large amplitude oscillatory shear was investigated using experiments and particle-level simulations. Under large amplitude oscillatory shear, an intensely oscillating normal stress was measured with a period of exactly half the strain period. As the amplitude of the strain increased, the peak of the normal stress increased and the trough decreased. Changes in the normal stress were mainly caused by two factors: the Poynting effect, in which shear produces a normal force perpendicular to the shear direction, and magnetic-induced normal stress, which changes with the particle structure. In MRPG, both effects are related to the particle structure. The particle structure in MRPG with different strain was calculated and the simulation results show that the amplitude of the structural strain in oscillatory shearing is less than that of the applied strain. Additionally, a phase difference was observed between the structural strain and the applied strain. Based on the calculated particle structure, the change in the normal stress was obtained and found to agree well with the experimental results. © *2018 The Society of Rheology.* https://doi.org/10.1122/1.5030952

I. INTRODUCTION

Magnetorheological polymer gels (MRPGs) are magneto-sensitive composites in which magnetizable particles are dispersed in a polymer gel [1,2]. Under a magnetic field, the particles rearrange themselves into chains along the direction of the magnetic field, whereupon interparticle magnetostatic interactions maintain the structure. When the material is subjected to external forces, the magnetic dipole force between particles can help resist deformation, and the magnetorheological (MR) effect can reach 1000% [3]. The magnetic dipole force between the particles is determined by the particle distribution, so the mechanical properties of MRPG are highly dependent on the particle structure.

The properties of viscoelastic materials are typically characterized by testing the shear stress during the oscillatory shear process, and then calculating the storage modulus and loss factor from the amplitude and phase shift of the shear stress [4–6]. As for MR materials, the particles rearrange themselves along the direction of the magnetic field, leading to an expanded stress [7–9]. As MR materials are often used in vibration isolation systems [10] and finishing [11,12], the normal stress generated during the shearing process has a great influence on the overall control effect. The normal stress in MR materials [13–15] has been intensively studied, with the main focus on the normal stress in squeeze mode [16–19]. Lopez-Lopez *et al*. theoretically studied the normal stresses in a shear flow of MR suspensions [20], deriving an expression for the normal stress that contains three terms. The first term comes from the tendency of the MR fluid to stretch along the magnetic field lines to decrease its magnetic energy. The second term is a result of magnetic field inhomogeneities, and the third term reflects the edge effect. de Vicente *et al*. studied the squeeze flow behavior of model MR fluids using a particle-level simulation methodology [18,21,22]. They also calculated the normal stress with different initial configurations and found that the particle structure had a big influence on the squeeze flow behavior. The influence of the particle structure on the performance of MR materials has been widely researched [23–25], and the results show that destroying the particle structure decreases the normal stress.

However, few researchers have studied the normal stress in MRPG during oscillatory shearing. Studying the normal stress in the process of oscillatory shearing allows us to examine the evolution of the particle structure. Additionally, changes in the normal stress in the process of oscillatory shear will produce an additional vibration source. Studying the normal stress may, therefore, be helpful for vibration reduction. The MRPG can be described as a biphasic system composed of a particle microstructure immersed in a viscous gel. Under large amplitude oscillatory shear, the particle structure is destroyed and reorganized. The obstruction of the rubber matrix means that the reorganization of the particle structure requires a certain amount of time. Studying the normal stress in the shearing process will enhance our knowledge of the particle structure, which will be helpful in analyzing the mechanical properties. For example, testing the normal stress during the shear process is beneficial to studying the phenomenon of shear thickening in MR fluids [26,27]. Additionally, as the normal stress of MRPG during shearing is very large (the same order of magnitude as the shear stress), understanding how the normal stress changes is of considerable interest. Besides, when a viscoelastic material

[a)]Author to whom correspondence should be addressed; electronic mail: gongxl@ustc.edu.cn

is sheared by twisting, an additional stress can be measured in the direction orthogonal to the shearing force [28,29], which complicates the changes in the normal stress.

This paper discusses the normal stress in MRPG under different shear modes, such as strain sweep, constant strain, and step strain. The macroscopic mechanical properties of the material are shown to be closely related to the particle microstructure. The particle structure in MRPG is simulated using a particle-level simulation methodology, and the corresponding magnetic-induced normal stress is also calculated. Finally, the effect of the Poynting effect and changes in the magnetic-induced normal stress are investigated. Based on the calculated particle structure, changes in the normal stress are obtained and found to be in good agreement with the experimental results.

II. EXPERIMENTAL

A. Sample preparation and experimental setup

The MRPG was prepared by dispersing carbonyl iron particles (CIP, type CN, provided by BASF in Germany with an average radius of 6 μm) into a homemade polyurethane (PU) gel. The polymer gel was synthesized by a chemical method. The materials used for the synthesis were toluene diisocyanate (TDI, 2,4-TDI at B80%, 2,6-TDI at B20%, Tokyo Chemical Industry Co., Ltd., Japan), polypropylene glycol (PPG-1000, $M_r = 1000$, Sinopec Group Co., Ltd., China), 1-methyl-2-pyrrolidone (Sinopharm Chemical Reagent Co., Ltd, China), and 1,4-butanediol (BDO, $M_r = 90$, Sinopharm Chemical Reagent Co., Ltd., China). To synthesize PU, the TDI and PPG were added to a flask at a molar ratio of 3:1 at 80 °C for 2 h. Their weights were calculated using the following formula:

$$\frac{m_{TDI}/174\,\mathrm{mol}^{-1}}{m_{PPG}/1000\,\mathrm{mol}^{-1}} = 3, \tag{1}$$

where m_{TDI} and m_{PPG} indicate the weights of TDI and PPG, and the numbers are the molecular weights of the compounds. BDO was later added to the reactor and the temperature was set to 60 °C. The weight of BDO was calculated by the following formula:

$$\frac{m_{TDI}/174\,\mathrm{mol}^{-1}}{\frac{m_{PPG}}{1000}\,\mathrm{mol}^{-1} + \frac{m_{BDO}}{90}\,\mathrm{mol}^{-1}} = 1.1. \tag{2}$$

After 30 min, 1-methyl-2-pyrrolidone was added to the mixture with a 10% weight ratio. The reaction was continuously stirred. Once the reaction was complete, the CIPs were added to the gel to give a CIP volume fraction of 20%. The prepared MRPG had a strong adhesion to the metal surface, so there was no wall slip phenomenon during the test (Fig. S1 [39]).

After preparing the MRPG, CIPs were uniformly dispersed in the PU matrix [Fig. S2(b) [39]] to form an isotropic sample. Under a magnetic field, the CIPs would rearrange themselves to form chain-like structures. Due to the hindrance of the matrix, the formation of the particle structure takes some time. To ensure that the particle structure in each sample was basically the same before the test, all samples were placed in a magnetic field for at least 300 s before testing. This process is called structuring. After the structuring process, the CIPs formed strings along the direction of the magnetic field, giving structured MRPG samples [Fig. S2(c) [39]]. Unless otherwise specified, the test samples were all structured MRPG. The mechanical properties of MRPG were tested by a commercial rheometer (Physica MCR302, Anton Paar GmbH, Austria) equipped with an electro-magnetic accessory (MRD180). A PP20 parallel-plate rotor was employed with a testing gap width of 1 mm. The current was set to 5 A (H = 950 kA/m). The normal stress, shear strain, and shear stress signals were also acquired by a dynamic signal analyzer (SignalCalc ACE, Data Physics Corp., USA) connected to the rheometer to collect more detailed information. The frequency of the signal acquisition was 125 Hz. To ensure the veracity of the data acquired by the dynamic signal analyzer, the normal stress tested by the rheometer was compared with that collected by the dynamic signal analyzer (Fig. S3 [39]). Fourier analysis (Fig. S4 [39]) was also used to eliminate the effects of transducer resonance or feedback [30]. The rheological properties of gels are also sensitive to many ambient factors [31], and so the reproducibility of the MRPG was tested (Fig. S5 [39]). To exclude the influence of other factors, samples were changed before each test in the experiment. In this study, the stress was defined as positive when the sample was pressed.

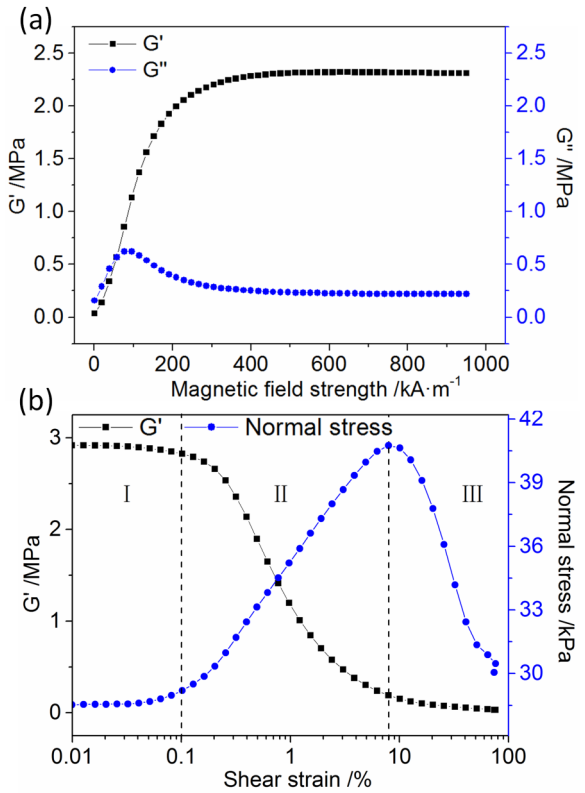

FIG. 1. Experimental results of the viscoelastic properties and normal stress in structured MRPG. (a) Storage modulus (G′) and loss modulus (G″) under different magnetic fields. (b) G′ and normal stress tested by the rheometer under different shear strains. The frequency during the strain sweep was 1 Hz and the magnetic field was 950 kA/m.

B. Normal stress under an oscillatory shear

Under a magnetic field, the CIPs in the MRPG were attracted to each other to produce a force that resisted shear. As shown in Fig. 1(a), G′ increased with the magnetic field and became saturated at ~400 kA/m. G″ first increased and then decreased with the increasing magnetic field and was much lower than G′ when the magnetic field was greater than 400 kA/m. Also, the chains of CIPs tended to stretch along the magnetic field lines to decrease their magnetic energy, which would lead to a normal stress. The normal stress in the MRPG was sufficiently large to be of the same order of magnitude as the shear stress. The magnetic-field-induced normal stress of MRPG was tested using the rheometer under different shear strains [Fig. 1(b)]. When the shear strain was less than 0.1%, the normal stress remained constant. The critical value of 0.1% formed the upper limit of the linear viscoelastic region. In this interval, the particle structure was unchanged. As the strain increased beyond this threshold, the normal stress increased significantly until reaching a maximum at a strain of 8%. After that, the normal stress decreased rapidly as the strain increased. With an increase in the strain, the particle structure is destroyed and the distance between CIPs increases, which will lead to a decrease in the normal stress. However, the normal stress was observed to increase in the second interval [Fig. 1(b)]. The normal stress varies in different sections with respect to the strain; this strain-dependent normal stress in MRPG has not previously been reported in the literature.

During the oscillatory shear, a complete oscillation period took 1 s ($f = 1$ Hz). The normal stress output from the rheometer was calculated over at least five cycles. To obtain detailed information about the normal stress over one oscillation cycle, a dynamic signal analyzer was connected to the rheometer to collect data from the force sensor. Figure 2 shows the real normal stress and normal stress tested by the rheometer during the strain sweep process. The normal stress tested by the dynamic signal analyzer was recorded as the real normal stress and the normal stress tested by the rheometer was recorded as the normal stress by rheometer. The strain increased exponentially from 1% to 100% in 40 s. The real normal stress was collected at a frequency of 125 Hz and the normal stress tested by the rheometer was the calculated value during every two cycles (in the test, record one point every 2 s, 2 cycles for 1 Hz.). Therefore, real normal stress could provide more specific information. Figure 2 clearly shows that the real change in normal stress was much greater than indicated by the rheometer, especially when the strain was greater than 10%. At a strain of less than 10%, the normal stress increased with strain, accompanied by an oscillation with the same frequency as the strain. The amplitude of the oscillatory normal stress also increased with the strain amplitude. When the strain reached ~10%, the oscillation of the normal stress was significantly aggravated. The peak of the normal stress reached twice the trough and 1.5 times the mean value. The minimum value of the oscillating normal stress continued to decrease until the strain reached 50%. After that, the normal stress became more stable. When the strain exceeded 10%, in addition to the significant increase in oscillation amplitude, the oscillation frequency doubled. In the oscillatory shearing process, the normal stress oscillates with strain because of the periodic disruption and reorganization of the particle structure. However, two other phenomena are difficult to interpret. The first is the different normal stress frequency at different strains, and the second is the increase in maximum normal stress with an increase in the amplitude of strain under large amplitude oscillatory shear.

C. Normal stress under constant shear strain amplitude

The results in Fig. 2 show that the oscillatory frequency of the normal stress started to double when the strain reached 10%. Therefore, the normal stress under oscillatory shear with constant amplitude was tested (Fig. 3). The normal stress in latter tests was the real shear stress recorded by the dynamic signal analyzer. The shape of the normal stress data changed with time. Over the first 20 s, the oscillatory frequency of the normal stress was equal to that of the shear strain. The difference was that the oscillation amplitude of the normal stress decreased. Figure 4 shows the strain and normal stress changes with respect to time at different time intervals. After 41 s, the disturbance is approximately equal

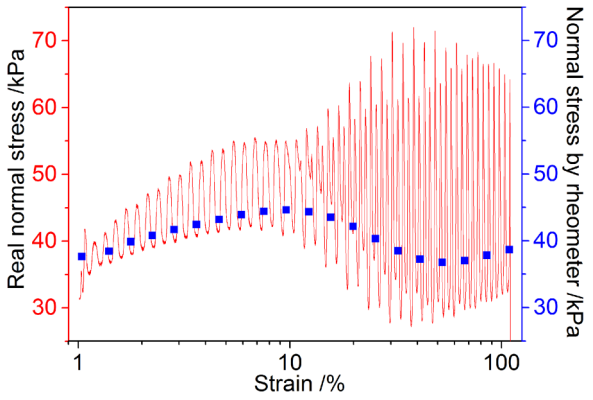

FIG. 2. Normal stress during the strain sweep process. The frequency was 1 Hz and the magnetic field was 950 kA/m. The normal stress tested by the dynamic signal analyzer was recorded as the real normal stress and the normal stress tested by the rheometer was recorded as the normal stress by rheometer.

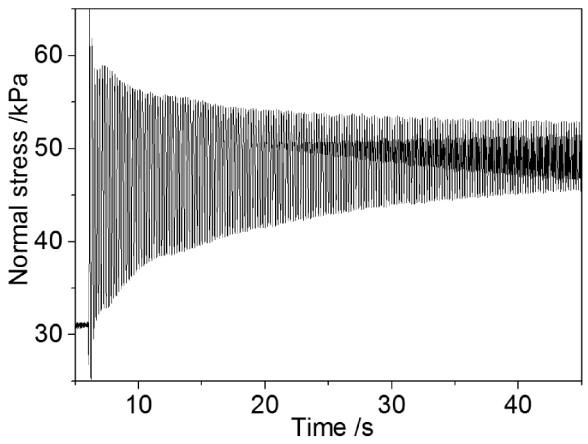

FIG. 3. Normal stress under oscillatory shear with constant strain amplitude. The amplitude of the oscillation shear was 10%, the frequency was 5 Hz, and the magnetic field was 950 kA/m.

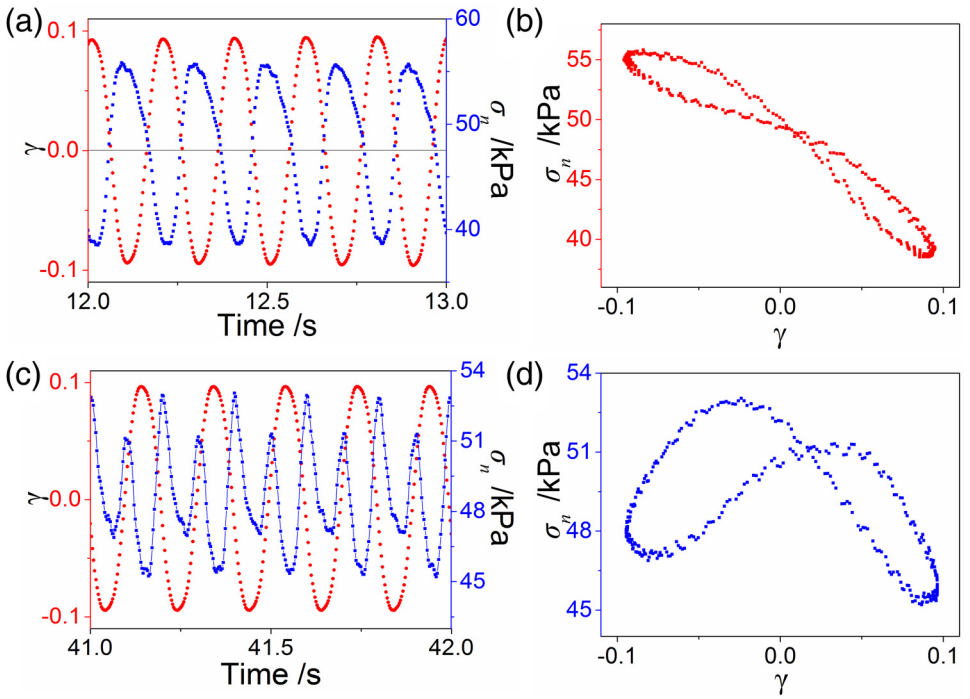

FIG. 4. Shear strain and normal stress with respect to time over different time intervals. (a) 12–13 s, (b) 41–42 s. Parts (b) and (d) show the Lissajous curves of normal stress versus shear strain from 12–13 s and 41–42 s, respectively.

to the original waveform. The frequency of the normal stress then doubled. Figure 4(d) shows the Lissajous curve of normal stress versus shear strain from 41 to 42 s. The shape of the curve has changed significantly compared with that in Fig. 4(b). The asymmetry of the earlier Lissajous image was caused by two factors. One was the initial asymmetric condition of the sample. That is, the sample was not completely symmetrical on the rheometer. The second factor might be the rheometer itself, as the process of applying shear might lead to asymmetry (Fig. S6 [39]). Asymmetry of the sample and asymmetric loading would result in the same normal stress frequency and shear frequency when the strain was smaller than 10% (Fig. S7 [39]). The normal stress in MRPG is mainly related to the particle structure. The change in the Lissajous curve indicates that, when the strain reaches 10%, the particle structure in the material will change over time. In later cases, at least 60 s of oscillatory shearing was applied before testing to stabilize the sample.

D. Normal stress under step strain

Under shear, some materials have a tendency to expand or shrink in the direction perpendicular to the applied shear stress, known as the Poynting effect [32]. The shear induced normal stress in a gel may be positive or negative [33,34]. At the same time, the doping particles influence the shear induced normal stress [35]. Therefore, the relationship between shear strain and normal stress in MRPG was experimentally studied. Figure 5(a) shows changes in the normal stress with respect to strain in isotropic MRPG and structured MRPG without applying a magnetic field. The isotropic MRPG is a sample that did not undergo a structuring process to distribute the CIPs evenly in the polymer matrix. The normal stress in this isotropic MRPG remained close to zero under increasing strain. However, the normal stress in the structured MRPG increased with the strain until the strain reached ∼10%, which demonstrates that the Poynting effect is related to the particle structure. At strains greater than 10%, the normal stress then decreased rapidly as the particle structure began to be destroyed. The critical strain is consistent with the results in Fig. 3. Experimental results indicate a positive normal stress in structured MRPG under shear, and this would increase with increasing strain until the strain reached ∼10%. However, as the strain increased further, the particle structure began to be destroyed, affecting the test results. To measure the exact normal stress under large strain, the normal stress was recorded under a step strain [Figs. 5(b)–5(d)]. The tested samples were structured MRPG, with a 950 kA/m magnetic field applied to better maintain the particle structure and allow convenient comparison with the previous results. The step strain means that a shear corresponding to a certain strain was applied to the sample as soon as possible. During the test, the rheometer took about 0.05–0.06 s to reach the set strain. As shown in Figs. 5(b)–5(d), as the strain increased, the normal stress first increased and then decreased rapidly before the strain reached its maximum value. When the step strain was 10%, the normal stress increased from 41 to 48 kPa in 0.03 s. The normal stress then decreased rapidly to a final value of ∼44 kPa, some 4 kPa greater than the initial value. This suggests that the chain-like structures were not completely destroyed. When the step strain reached 50%, the normal stress increased by ∼28 kPa in 0.01 s, and the maximum normal stress reached ∼70 kPa, the same as the maximum normal stress in Fig. 2. This explains why the maximum stress increased with the strain in Fig. 2. The normal stress then decreased due to the increase in particle

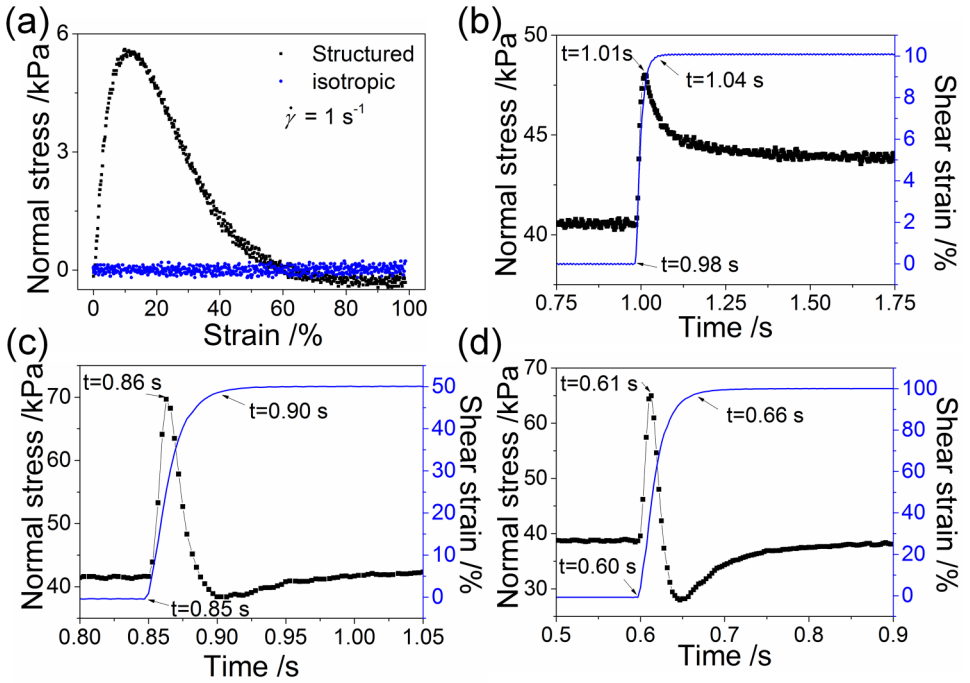

FIG. 5. Normal stress in MRPG under step strain. (a) Normal stress versus shear strain. The strain increased from 0% to 100% within 1 s and the strain rate was 1 s^{-1}. The normal stress in the shearing process was tested without a magnetic field. (b)–(d) Normal stress and shear strain versus time under step strain; the strain was set to 10%, 50%, and 100% in turn. A 950 kA/m magnetic field was applied to the structured MRPG.

distance, and a trough appeared after the increase in the normal stress. The final stress is the same as the initial value, indicating that the particle structure has been destroyed and reorganized. As the strain continued to increase, the normal stress remained constant [Fig. 5(d)], indicating that the Poynting effect only operates over a certain range. At this point, we can conclude that the Poynting effect in structured MRPG is related to the friction and squeezing between particles when the sample is sheared. Increasing the shear strain, the squeezing effect between the particles becomes more obvious, and the normal stress increases. As the strain continues to increase, the interparticle space increases and the normal stress caused by the Poynting effect rapidly decreases.

During the oscillatory shear, the maximum normal stress increases with the strain under the Poynting effect, and the minimum normal stress decreases as the particle structure is broken down and the magnetic-induced normal stress decreases. At this point, we can conclude that the changes in normal stress during the process of oscillatory shear are mainly caused by two factors: the magnetic-induced normal stress caused by the change of particle structure during shear and the Poynting effect in anisotropic materials. Both of these factors depend on the evolution of the particle structure in the MRPG.

III. PARTICLE-LEVEL DYNAMIC SIMULATION

A. Particle–particle interactions and kinematic equation

When an iron particle with a diameter d_i is placed in a uniform magnetic field $\boldsymbol{H}$ (Fig. 6), the magnetic moment $\boldsymbol{m}_i$ of the particle is

$$\boldsymbol{m}_i = \boldsymbol{m}_s(1 - e^{-\chi H})V, \tag{3}$$

where $\boldsymbol{m}_s$ is the saturated magnetization of the iron particle, $V = \pi d_i^3/6$ is the volume of particle i, and χ is the adaptive magnetization coefficient. Using experimental data [36], we fixed $\boldsymbol{m}_s = 6.9 \times 10^5$ A/m and $\chi = 5.06 \times 10^{-6}$ m/A.

The dipole force between two CIPs is given by

$$\boldsymbol{F}_{ij}^{m} = \begin{cases} c_m \times \boldsymbol{F}_{ij}^{dipole}, & \text{for } D \le r \le 1.5D \\ \boldsymbol{F}_{ij}^{dipole}, & \text{for } r > 1.5D, \end{cases} \tag{4}$$

$$\boldsymbol{F}_{ij}^{dipole} = -\frac{3\mu_0}{4\pi\mu_f r_{ij}^4}[\boldsymbol{m}_i \cdot \boldsymbol{m}_j\hat{\boldsymbol{r}} + \boldsymbol{m}_i \cdot \hat{\boldsymbol{r}}\boldsymbol{m}_j + \boldsymbol{m}_j \cdot \hat{\boldsymbol{r}}\boldsymbol{m}_i - 5(\boldsymbol{m}_i \cdot \hat{\boldsymbol{r}})(\boldsymbol{m}_j \cdot \hat{\boldsymbol{r}})\hat{\boldsymbol{r}}], \tag{5}$$

$$c_m = 1 + \left(3 - \frac{2r_{ij}}{d_{ij}}\right)^2 \left(\frac{60.17}{1 + e^{\dfrac{\theta - 34.55}{12.52}}} - 22.79\right) \Big/ 100, \tag{6}$$

where $\boldsymbol{r}$ is the position vector from particle i to particle j and $r = |\boldsymbol{r}|$, $\hat{\boldsymbol{r}} = \boldsymbol{r}/r$. c_m is the correction factor for adjusting a

magnetic point dipole to model two close magnetized iron particles [36]. d_{ij} is the average diameter of the two particles.

To avoid the magnetized particles overlapping, the excluded volume force $\boldsymbol{F}_{ij}^{ev}$ was introduced. This force, calculated by Melle *et al.* [37] as

$$\boldsymbol{F}_{ij}^{ev} = -\frac{3\mu_0 \boldsymbol{m}_i^s \boldsymbol{m}_j^s}{2\pi d_{ij}^4} e^{-10\left(\frac{r_{ij}}{d_{ij}}-1\right)} \hat{\boldsymbol{r}}_{i,j}, \tag{7}$$

balances the magnetic force when two particles are in contact and $\boldsymbol{m}_i^s = \boldsymbol{m}_s V_i$.

The interparticle van der Waals force can be expressed as [38]

$$\boldsymbol{F}_{ij}^{vdw} = \frac{A}{24}\frac{d_{ij}}{L_r^2}\hat{\boldsymbol{r}}, \tag{8}$$

where $A = 5\times10^{-19}$ J is the Hamaker constant and $L_r = \max[r_{ij} - d_{ij},\ 0.001 d_{ij}]$.

In both simulations and experiments, the motion of particles related to the Bingham fluid has an extremely low Reynolds number. Hence, the hydrodynamic drag force is

$$\boldsymbol{F}_i^d = -\frac{19}{8}\pi(\tau_0 d_i^2 \hat{\boldsymbol{v}} + d_i \eta \boldsymbol{v}), \tag{9}$$

where τ_0 is the shear yield stress of the matrix and $\hat{\boldsymbol{v}}$ is the unit vector of velocity relative to the surrounding matrix. The resultant gravity and buoyancy forces acting on a particle can be expressed as

$$\boldsymbol{F}_i^g = \frac{\pi d_i}{6}(\rho - \rho_m)\boldsymbol{g}, \tag{10}$$

where ρ and ρ_m are the densities of the particle and the matrix, respectively, and $\boldsymbol{g}$ is the gravitational acceleration. As CIP is a soft magnetic material, the magnetic torque applied on the particles is so small that the magneto-induced body rotational motion of the iron particles can be neglected. In addition, the inertia effect and stochastic motion of the particles have not been taken into account. Considering the aforementioned interactions, the kinematic equation can be constructed as

$$\frac{\mathrm{d}\boldsymbol{r}_i}{\mathrm{d}t} = \begin{cases} 0, & \text{for } |\sum F_i| \le \frac{19}{8}\pi\tau_0 \mathrm{d}_i^2, \\ \frac{8}{19\pi \mathrm{d}_i \eta}\left\{\begin{array}{l}\sum\limits_{j\neq i}(\boldsymbol{F}_{ij}^m + \boldsymbol{F}_{ij}^{ev} + \boldsymbol{F}_{ij}^{vdw}) \\ +\boldsymbol{F}_i^g - \frac{19}{8}\pi\tau_0 \mathrm{d}_i^2 \hat{\boldsymbol{v}}\end{array}\right\}, & \text{for } |\sum F_i| > \frac{19}{8}\pi\tau_0 \mathrm{d}_i^2, \end{cases} \tag{11}$$

where $\sum F_i$ denotes the total force, excluding the hydrodynamic drag force, on particle i. Equation (11) can be solved using a numerical method. The basic parameters are given in the supplementary material (Fig. S9) [39]. The particle structure can then be calculated.

A sinusoidal shear is then applied to the simulation cell. The strain is divided into many time steps, with a small strain applied in each step. In the simulation, the time step $dt = 1$ ms. In each time interval, the coordinates of the particle position are corrected according to the strain, and then Eq. (11) is resolved until the strain reaches the set point. Once the particle position has been determined, the angle and force between particles can be calculated. The normal component of the dipole force between two particles is

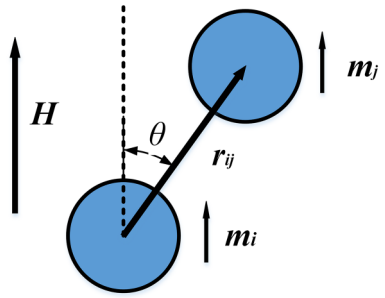

FIG. 6. Schematic diagram of each parameter used in the simulation.

$$F_{ij}^z = \frac{3\mu_0}{4\pi\mu_f r_{ij}^4}(5m_i m_j \cos^2\theta - 3m_i m_j)\cos\theta, \tag{12}$$

and the normal stress is

$$\sigma_{zz} = \frac{1}{V_c}\sum_{i=1}^{N-1}\sum_{j=i+1}^{N} z_{ij} F_{ij}^z, \tag{13}$$

where θ is the angle between two particles and V_c is the volume of the considered cell. F_{ij}^z decreases with increasing θ, meaning that the normal stress will decrease with increasing strain.

B. Normal stress and particle structure under shear

Figure 7 shows the calculated magnetic-induced normal stress under an increasing strain in MRPG. As the strain increases, the normal stress remains almost constant, albeit slightly increasing, when the strain is less than ~10%. As the strain increases above this point, the normal stress decreases rapidly. The critical strain is consistent with the results in Fig. 2. When the strain exceeded 80%, there was a slight

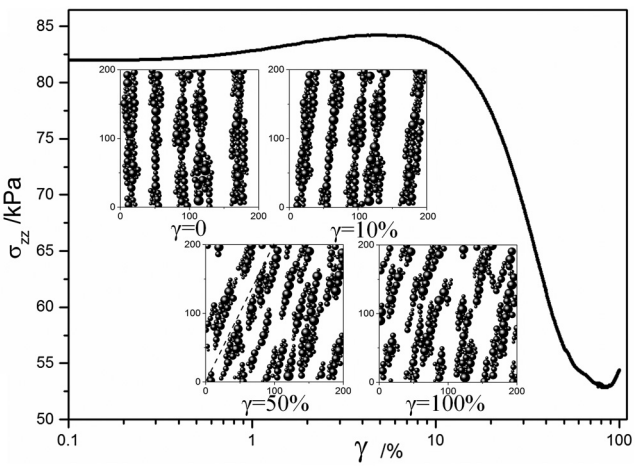

FIG. 7. Calculated magnetic-induced normal stress σ_{zz} and particle structure in MRPG under different shear strains. The figure shows the results in the first quarter of the sinusoidal shear.

increase in the normal stress. Combined with the particle structure in Fig. 7, this indicates that when the strain is less than 10%, the particle structure is tilted by the strain and the angle of the particle chain is the same as the strain. The chain-like structure has not been destroyed, and so the normal stress is basically unchanged. When the strain reached 50%, many particle chains were interrupted, leading to a reduction in the normal stress. The results also suggest that the slope angle of the particle chain is smaller than the angle corresponding to the applied strain. With the inclination of the particle chains, the potential energy between the particles increases and the particle chains recombine to decrease the potential energy. As the strain increased further, the shear rate decreased and the reorganization of the particle structure occurred faster than its destruction. The angle of the particle chains decreased, resulting in a slight increase in normal stress. The internal particle structure changed with strain, and the strain of the particle structure deviated from the applied strain. The evolution of the particle structure over time could then be calculated.

The angle probability distribution $P(\theta)$, which represents the probability of the angle between two particles being θ, was calculated in MRPGs with different particle structures according to

$$P(\theta) = \frac{N(\theta)}{N_{\text{total}}}, \tag{14}$$

where θ represents the angle between the line connecting the particles and the z axis. $N(\theta)$ represents the number of angles equal to θ and N_{total} represents the total number of possible angles within the calculation area. The angle between two particles with an interparticle distance of less than some cutoff radius was examined. In the simulation, the cutoff radius was set to 1.5 times the average diameter of the two particles. As shown in Fig. 8, after prestructuring, the particle chains lay along the direction of the magnetic field. The most probable angle and the average angle were 0°, representing the direction perpendicular to the shear. After 10 cycles of oscillatory shear, the strain of the sample was zero, but the most probable angle in the particle structure was 18°. To further explore changes in the particle structure under oscillatory shear, the average angles were used to represent the strain of the particle structure. Based on Figs. 7 and 8, we can conclude that there is a phase difference between the strain of the particle structure and the applied strain. The amplitude of the structural strain is also less than that of the applied strain.

To further understand the changes in the normal stress, the strain of the particle structure and the normal stress in each oscillation cycle was calculated. As shown in Fig. 9, the strain of the particle structure also oscillated over time, with an oscillation amplitude of 0.2. Here, the average of the angle between two particles was used to represent the strain of the particle structure called the structural strain. This was less than the most probable angle. The strain of the particle structure was found to be nonzero under no applied shear strain and did not attain its maximum when the strain was at its highest. However, the strain of the structure changed periodically and was symmetrical, with the same cycle as that of the applied strain. According to Eqs. (12) and (13), the magnitude of normal stress depends only on the magnitude of the strain and not its direction. Therefore, the frequency of the normal stress is twice the strain frequency. In addition, the phase difference between the structural strain and the applied strain will cause a difference in the shape of the stress–strain relation illustrated in the Lissajous curve. Thus, Lissajous curves were used to study the influence of the strain amplitude and shear frequency on the normal stress.

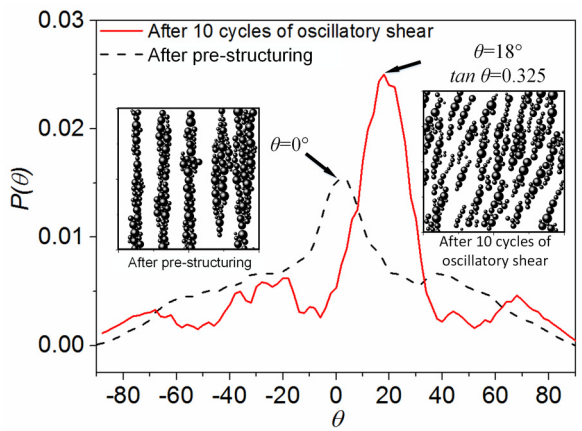

FIG. 8. Angle probability distribution in MRPGs with different particle structures. Black dotted line: after prestructuring, red solid line: after 10 cycles of oscillatory shear. The strain amplitude is 100%.

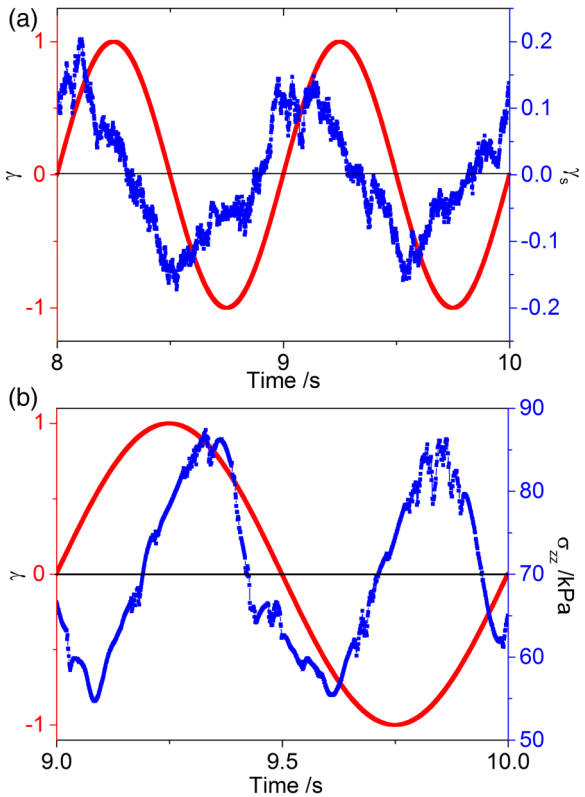

FIG. 9. Strain of the particle structure and normal stress in MRPG under oscillatory shear. (a) Applied shear strain γ and the strain of the particle structure γ_s versus time and (b) γ and calculated magnetic-induced normal stress σ_{zz} versus time. The frequency was 1 Hz, $\gamma = 100\%$, and the magnetic field was 950 kA/m.

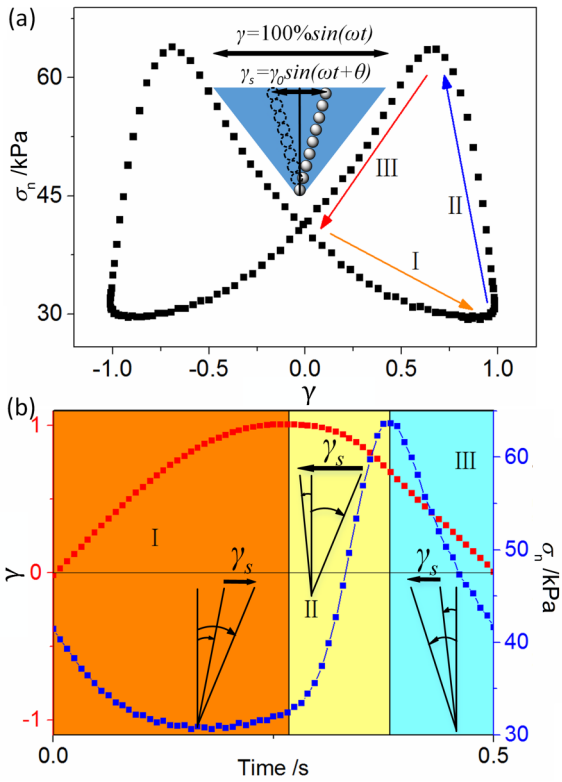

FIG. 10. Variation of normal stress with strain in computational simulations and experiments. (a) Lissajous curve of normal stress versus shear strain. The strain was expressed as $\gamma = 100\%\sin(\omega t)$ and the strain of the particle structure was roughly expressed as $\gamma_s = \gamma_0\sin(\omega t + \varphi)$, where γ_0 is less than 100%. The normal stress can be divided into three regions according to the strain changes. (b) Structural strain changes with the applied strain and normal stress changes with time. The normal stress and shear strain are experimental results, and the structural strain is the calculated result.

IV. RESULTS AND DISCUSSION

Experimental tests demonstrated that the normal stress increased with increasing strain because of the Poynting effect present in MRPGs with chain-like structures. The particle structure was simulated during the oscillatory shear process, and the relationship between the magnetic-induced normal stress and the structural strain was also calculated. Changes in the normal stress with respect to the strain could then be approximately deduced. As shown in Fig. 10(a), when the applied strain was $\gamma = 100\%\sin(\omega t)$, the strain of the particle structure could be approximated as $\gamma_s = \gamma_0\sin(\omega t + \varphi)$, where φ represents the phase difference and γ_0 is less than 100%. The Lissajous curve of normal stress versus shear strain had a symmetrical, butterfly-like shape, and the area enclosed by the curve was related to the phase difference. Because of the left and right symmetry of the curve, the stress could be divided into three intervals according to the strain changes. Figure 10(b) shows the variation in structural strain as the normal stress changes. In the first interval, the structural strain increased with increasing shear strain, leading to a decrease in the normal stress. When the shear strain reached its maximum, the normal stress increased slightly due to the reduction of the shear rate and the reorganization of the chain-like structure. In this area, the structural strain was large, the interparticle space increased, and the chain-like structure was destroyed. As a result, the Poynting effect could not be observed. In the second interval, as the strain decreased, the structural strain decreased rapidly until it reversed. The magnetic-induced normal stress increased and the CIPs in the MRPG formed a chain-like structure. With the increase of strain in the reverse direction, the magnetic-induced normal stress remained almost constant (the structural strain was less than 10%), but the total normal stress increased because of the Poynting effect. In the third interval, as the strain continued to increase, the chain-like structure was destroyed and the Poynting effect diminished. The magnetic-induced normal stress reduced with the increasing structural strain, causing the normal stress to decrease. During the whole process, the close relationship between the Poynting effect and the particle structure made it difficult to quantify the normal stress caused by different levels of strain. That is, the continuous change in the particle

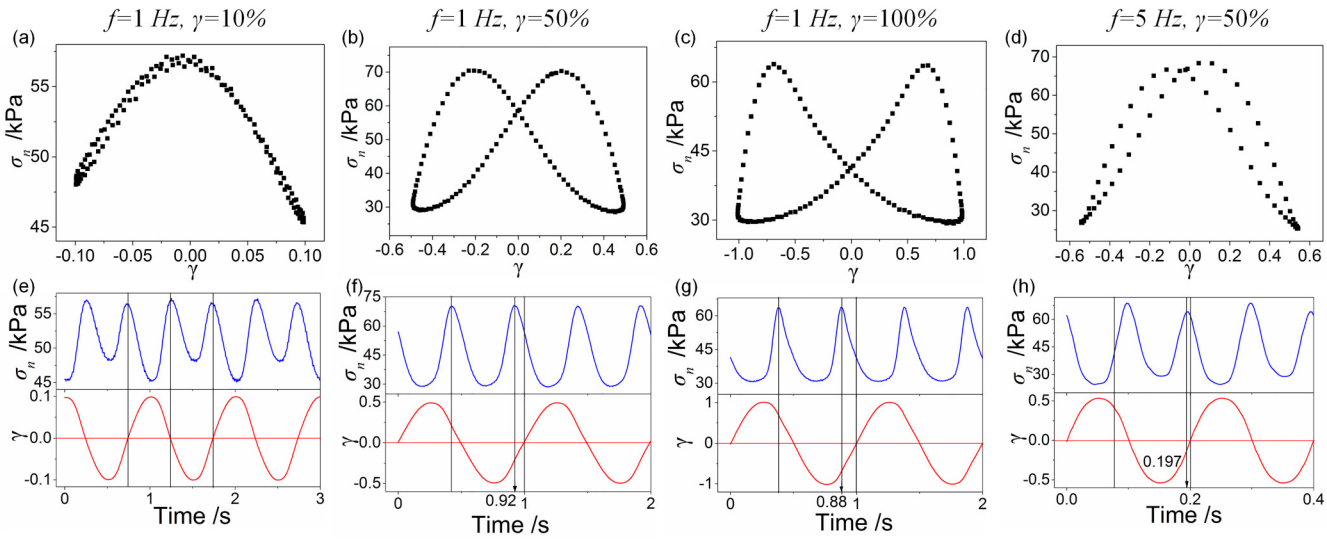

FIG. 11. Normal stress tested at different oscillatory strain and frequencies. (a)–(d) show the Lissajous curves of normal stress versus shear strain and (d)–(f) show the corresponding time dependent normal stress and applied shear strain. All data were stable after at least 60 s oscillation shear and the magnetic field was 950 kA/m.

structure during the oscillatory shear made it difficult to quantitatively describe the changes in normal stress. However, the area enclosed by the Lissajous curve was clearly related to the phase difference between the structural strain and the applied strain. Thus, the influence of the strain amplitude and frequency on the phase difference was studied.

The Lissajous curves of normal stress versus shear strain were plotted under different oscillatory strains and frequencies. As the strain increased, there was a clear change in the Lissajous curves. When the strain increased, the variation range of the normal stress increased. After the strain exceeded 50%, the variation range of the normal stress remained unchanged, but the area enclosed by the curve continued to increase. The areas enclosed by the curves represent the phase differences between normal stress and shear strain, with a larger area corresponding to a larger phase difference. Therefore, the phase difference between the normal stress and strain clearly increased as the oscillating strain increased. An increase in the applied strain also caused the structural strain to increase. As a result, the magnetic dipole force acting on the particle chain increased, and the phase difference between the applied strain and the structural strain increased. The oscillation frequency also has a strong influence on the phase difference between normal stress and shear strain. Comparing Figs. 11(b) and 11(d), it is apparent that the phase difference decreases as the frequency increases. The particle structure requires a certain amount of time to form. Increasing the frequency shortens the particle structure recombination time, reducing the phase difference between normal stress and shear strain. As a result, the phase difference between the structural strain and the applied strain increases with increasing strain and decreases with increasing frequency. Thus, the influence of the strain amplitude and frequency on the phase difference between the structural strain and the applied strain can be obtained, which is helpful when analyzing the viscoelastic properties of the material.

V. CONCLUSION

In this study, the normal stress in MRPG during oscillatory shear was studied by both experimental tests and numerical simulations. The results showed that, in the process of oscillatory shearing, a continued increase in the strain divided the normal stress curve into three intervals. In the linear viscoelastic region ($\gamma < 0.1\%$), the normal stress was basically unchanged. In the second interval ($0.1\% < \gamma < 8\%$), the mean normal stress increased with the increasing strain. From this point, the normal stress exhibited obvious oscillations with the same frequency as the oscillatory shearing. In the third interval ($8\% < \gamma < 100\%$), the normal stress decreased with increasing strain, but the variations were somewhat complicated. In this interval, the oscillation of the normal stress was more intense. As the strain increased, the maximum value of the normal stress increased and the minimum value decreased. The frequency of the normal stress became twice the shear frequency. Through experimental testing of MRPG samples under oscillatory shear with different loading modes and computer simulations of the particle structure in the MRPG, two main reasons for the change in normal stress were identified. One was the Poynting effect in MRPGs with chain-like particle structures, and the other was the change of magnetic-induced normal stress according to the particle structure. The combination of the two effectively explains the experimental results. As the strain of the particle structure increased, the normal stress would increase due to the Poynting effect, but the magnetic-induced normal stress would decrease as the chain-like structure in the MRPG was destroyed and the interparticle distance increased. The maximum value of the normal stress during the oscillatory shear was then determined by the Poynting effect and the minimum value depended on the amplitude of the structural strain. The calculated results indicate a phase difference between the structural strain and the applied strain. Lissajous curves of normal stress versus shear strain were plotted at different shear strains and shear frequencies. The phase difference between the normal stress and the applied strain could then be calculated from the area enclosed by the curve, allowing the influence of strain amplitude and frequency on this phase difference to be determined. Further study is needed to elucidate the relationship between the Poynting effect and the particle structure.

ACKNOWLEDGMENTS

Financial support from the National Natural Science Foundation of China (Grant No. 11572309) and the Strategic Priority Research Program of the Chinese Academy of Sciences (Grant No. XDB22040502) are gratefully acknowledged. This work is also supported by the Collaborative Innovation Center of Suzhou Nano Science and Technology.

References

[1] Mitsumata, T., and N. Abe, "Magnetic-field sensitive gels with wide modulation of dynamic modulus," Chem. Lett. **38**(9), 922–923 (2009).

[2] Wilson, M. J., A. Fuchs, and F. Gordaninejad, "Development and characterization of magnetorheological polymer gels," J. Appl. Polym. Sci. **84**(14), 2733–2742 (2002).

[3] Xu, Y. G., X. L. Gong, S. H. Xuan, W. Zhang, and Y. C. Fan, "A high-performance magnetorheological material: preparation, characterization and magnetic-mechanic coupling properties," Soft Matter **7**(11), 5246–5254 (2011).

[4] Shkel, Y. M., and D. J. Klingenberg, "A thermodynamic approach to field-induced stresses in electro- and magnetoactive composites," Int. J. Mod. Phys. B **15**(6-7), 795–802 (2001).

[5] Kim, P., J.-I. Lee, and J. Seok, "Analysis of a viscoplastic flow with field-dependent yield stress and wall slip boundary conditions for a magnetorheological (MR) fluid," J. Non-Newtonian Fluid Mech. **204**, 72–86 (2014).

[6] Laun, H. M., C. Gabriel, and C. Kieburg, "Wall material and roughness effects on transmittable shear stresses of magnetorheological fluids in plate-plate magnetorheometry," Rheol. Acta **50**(2), 141–157 (2011).

[7] Pessot, G., H. Loewen, and A. M. Menzel, "Dynamic elastic moduli in magnetic gels: Normal modes and linear response," J. Chem. Phys. **145**(10), 104904 (2016).

[8] Jiang, J., Y. Tian, D. Ren, and Y. Meng, "An experimental study on the normal stress of magnetorheological fluids," Smart Mater. Struct. **20**(8), 085012 (2011).

[9] Yao, X., M. Yu, and J. Fu, "Magnetic-enhanced normal force of magnetorheological fluids," Smart Mater. Struct. **24**(3), 035001 (2015).

[10] Yazid, I. I. M., S. A. Mazlan, F. Imaduddin, H. Zamzuri, S. B. Choi, and T. Kikuchi, "An investigation on the mitigation of end-stop impacts in a magnetorheological damper operated by the mixed mode," Smart Mater. Struct. **25**(12), 125005 (2016).

[11] Lambropoulos, J. C., C. Miao, and S. D. Jacobs, "Magnetic field effects on shear and normal stresses in magnetorheological finishing," Opt. Express **18**(19), 19713–19723 (2010).

[12] Esmaeilzare, A., S. M. Rezaei, and B. Ramezanzadeh, "Corrosion and magnetic properties of encapsulated carbonyl iron particles in aqueous suspension by inorganic thin films for magnetorheological finishing application," Appl. Surf. Sci. **436**, 1200–1212 (2018).

[13] Liu, T., Y. Xu, X. Gong, H. Pang, and S. Xuan, "Magneto-induced normal stress of magnetorheological plastomer," AIP Adv. **3**(8), 082122 (2013).

[14] Ju, B. X., M. Yu, J. Fu, X. Zheng, and S. Z. Liu, "Magnetic field-dependent normal force of magnetorheological gel," Ind. Eng. Chem. Res. **52**(33), 11583–11589 (2013).

[15] Liao, G., X. Gong, S. Xuan, C. Guo, and L. Zong, "Magnetic-field-induced normal force of magnetorheological elastomer under compression status," Ind. Eng. Chem. Res. **51**(8), 3322–3328 (2012).

[16] de Vicente, J., F. Gonzalez-Caballero, G. Bossis, and O. Volkova, "Normal force study in concentrated carbonyl iron magnetorheological suspensions," J. Rheol. **46**(5), 1295–1303 (2002).

[17] Kordonski, W., and S. Gorodkin, "The behavior of a magnetorheological (MR) fluid under compressive deformation," J. Rheol. **60**(1), 129–139 (2016).

[18] Ruiz-Lopez, J. A., Z. W. Wang, R. Hidalgo-Alvarez, and J. de Vicente, "Simulations of model magnetorheological fluids in squeeze flow mode," J. Rheol. **61**(5), 871–881 (2017).

[19] Chen, P., L.-J. Qian, X.-X. Bai, and S.-B. Choi, "Velocity-dependent characteristics of magnetorheological fluids in squeeze mode considering the hydrodynamic and the magnetic field interactions," J. Rheol. **61**(3), 455–465 (2017).

[20] Lopez-Lopez, M. T., P. Kuzhir, J. D. G. Duran, and G. Bossis, "Normal stresses in a shear flow of magnetorheological suspensions: Viscoelastic versus Maxwell stresses," J. Rheol. **54**(5), 1119–1136 (2010).

[21] de Vicente, J., J. A. Ruiz-Lopez, E. Andablo-Reyes, J. P. Segovia-Gutierrez, and R. Hidalgo-Alvarez, "Squeeze flow magnetorheology," J. Rheol. **55**(4), 753–779 (2011).

[22] Ruiz-Lopez, J. A., R. Hidalgo-Alvarez, and J. de Vicente, "A micromechanical model for magnetorheological fluids under slow compression," Rheol. Acta **55**(3), 215–221 (2016).

[23] Kuzhir, P., M. T. Lopez-Lopez, G. Vertelov, C. Pradille, and G. Bossis, "Shear and squeeze rheometry of suspensions of magnetic polymerized chains," Rheol. Acta **47**(2), 179–187 (2008).

[24] Rodriguez-Lopez, J., P. Castro Blazquez, L. Elvira, F. Montero de Espinosa, J. Ramirez, and J. de Vicente, "On the yielding behaviour in magnetorheology using ultrasounds, shear and normal stresses, and optical microscopy," J. Phys. D: Appl. Phys. **48**(46), 465503 (2015).

[25] Zubarev, A. Y., D. N. Chirikov, D. Y. Borin, and G. V. Stepanov, "Hysteresis of the magnetic properties of soft magnetic gels," Soft Matter **12**(30), 6473–6480 (2016).

[26] Tian, Y., J. Jiang, Y. Meng, and S. Wen, "A shear thickening phenomenon in magnetic field controlled-dipolar suspensions," Appl. Phys. Lett. **97**(15), 151904 (2010).

[27] Bossis, G., Y. Grasselli, A. Meunier, and O. Volkova, "Outstanding magnetorheological effect based on discontinuous shear thickening in the presence of a superplastifier molecule," Appl. Phys. Lett. **109**(11), 111902 (2016).

[28] Labiausse, V., R. Hohler, and S. Cohen-Addad, "Shear induced normal stress differences in aqueous foams," J. Rheol. **51**(3), 479–492 (2007).

[29] Pan, Z. C., H. de Cagny, M. Habibi, and D. Bonn, "Normal stresses in shear thickening granular suspensions," Soft Matter **13**(20), 3734–3740 (2017).

[30] Poulos, A. S., F. Renou, A. R. Jacob, N. Koumakis, and G. Petekidis, "Large amplitude oscillatory shear (LAOS) in model colloidal suspensions and glasses: frequency dependence," Rheol. Acta **54**(8), 715–724 (2015).

[31] Aktas, S., D. M. Kalyon, B. M. Marin-Santibanez, and J. Perez-Gonzalez, "Shear viscosity and wall slip behavior of a viscoplastic hydrogel," J. Rheol. **58**(2), 513–535 (2014).

[32] Poynting, J. H., "On pressure perpendicular to the shear planes in finite pure shears, and on the lenghtening of loaded wires when twisted," Proc. R. Soc. Lond. A **82**(557), 546–559 (1909).

[33] Janmey, P. A., M. E. Mccormick, S. Rammensee, J. L. Leight, P. C. Georges, and F. C. Mackintosh, "Negative normal stress in semiflexible biopolymer gels," Nat. Mater. **6**(1), 48–51 (2007).

[34] de Cagny, H. C. G., B. E. Vos, M. Vahabi, N. A. Kurniawan, M. Doi, G. H. Koenderink, F. C. MacKintosh, and D. Bonn, "Porosity governs normal stresses in polymer gels," Phys. Rev. Lett. **117**(21), 217802 (2016).

[35] Adkins, J. E., and R. S. Rivlin, "Large elastic deformations of isotropic materials. 10. Reinforcement by inextensible cords," Philos. Trans. R. Soc. Lond. A **248**(944), 201–223 (1955).

[36] Liu, T. X., X. L. Gong, Y. G. Xu, S. H. Xuan, and W. Q. Jiang, "Simulation of magneto-induced rearrangeable microstructures of magnetorheological plastomers," Soft Matter **9**(42), 10069–10080 (2013).

[37] Melle, S., O. G. Calderon, M. A. Rubio, and G. G. Fuller, "Rotational dynamics in dipolar colloidal suspensions: video microscopy experiments and simulations results," J. Non-Newtonian Fluid Mech. **102**(2), 135–148 (2002).

[38] Klingenberg, D. J., C. H. Olk, M. A. Golden, and J. C. Ulicny, "Effects of nonmagnetic interparticle forces on magnetorheological fluids," J. Phys. Condens. Matter **22**(32), 324101 (2010).

[39] See the supplementary material at https://doi.org/10.1122/1.5030952 for the adhesion performance, particle structure, repeatability, Fourier rheology spectrum, normal stress with angles of structuration, and calculation parameters of MRPG.